
Geometry-Aware Normalizing Wasserstein Flows for Optimal Causal Inference

Kaiwen Hou
Columbia Business School

Abstract

This manuscript enriches the framework of continuous normalizing flows (CNFs) within causal inference, primarily to augment the geometric properties of parametric submodels used in targeted maximum likelihood estimation (TMLE). By introducing an innovative application of CNFs, we construct a refined series of parametric submodels that enable a directed interpolation between the prior distribution p_0 and the empirical distribution p_1 . This proposed methodology serves to optimize the semiparametric efficiency bound in causal inference by orchestrating CNFs to align with Wasserstein gradient flows. Our approach not only endeavors to minimize the mean squared error in the estimation but also imbues the estimators with geometric sophistication, thereby enhancing robustness against misspecification. This robustness is crucial, as it alleviates the dependence on the standard $n^{\frac{1}{4}}$ rate for a doubly-robust perturbation direction in TMLE. By incorporating robust optimization principles and differential geometry into the estimators, the developed geometry-aware CNFs represent a significant advancement in the pursuit of doubly robust causal inference.

process. Nonetheless, the efficiency of TMLE hinges on the precise definition of the perturbation direction, which in turn is contingent on the accuracy of the specified propensity models—a requirement often strenuous to fulfill in practice.

Our contribution lies in the application of continuous normalizing flows (CNFs) to enrich the geometric delineation of these parametric submodels within the TMLE framework. CNFs, with their capacity for complex distribution modeling through a differential equation framework, introduce a heightened level of flexibility and geometric awareness to the estimation process. Specifically, our technique contrasts with traditional TMLE by embarking on a path that minimizes the Cramér-Rao bound from a priori knowledge encapsulated in p_0 towards an empirically-informed distribution p_1 .

We extend the typical use of CNFs, which often relies on Fokker-Planck equations to describe probabilistic transitions, by employing Wasserstein gradient flows. This empowers a more efficient and acute navigation through the space of models, attentive to the evolution of density functions.

Drawing from the theoretical work of Chen et al. (2018), we assert that while Fokker-Planck equations provide a robust theoretical foundation for such transformations, the incorporation of Wasserstein gradient flows caters to a more functional and specific implementation in the context of causal inference. This perspective allows us to bypass the limitations identified by Liu et al. (2022) and Raissi et al. (2019) related to the parametrization of these equations, fostering a CNFs utilization that is more informed and structurally sound. Consequently, our approach enables an estimation that is both nuanced and geometrically congruent, aligning well with the intricate requirements of causal inference.

Furthermore, the versatility of CNFs permits the imposition of additional structures or criteria based on prior objectives. If the true distribution is suspected to reside within a particular manifold of statistical sub-

1 INTRODUCTION

The fidelity of causal effect estimates is substantially influenced by the underlying statistical models in the field of causal inference. TMLE, a pivotal methodology in this domain, utilizes a series of parametric submodels to converge towards the true data-generating

models, our methodology can constrain the flow transformations to honor this geometric structure. This approach transcends regularization, becoming a pivotal element for enhancing model robustness, such as by integrating optimal transport theory into the transformations.

Acknowledging the numerical tractability of instantaneous changes of variables in CNFs, as noted by Chen et al. (2018), we also address the challenge presented by neural network parameterizations of the Fokker-Planck equations, which traditionally depend on sampling methods. Inspired by the innovation in physics-informed neural networks (Raissi et al., 2019), our paper advocates for a sophisticated embedding of the functional forms of the PDE within CNFs, bolstering their application in causal analysis.

2 PRELIMINARIES

This section presents an overview of the general formulation of Wasserstein gradient flows, detailing their interrelation with continuous normalizing flows.

2.1 2-Wasserstein metric

Consider a Radon space $(\mathcal{P}(\Omega), \mathcal{W}_2)$ where $\mathcal{P}(\Omega)$ denotes the set of probability measures on a compact sample space Ω , and \mathcal{W}_2 represents the 2-Wasserstein metric

$$\mathcal{W}_2(\mu, \nu) = \left(\inf_{\gamma \in \Gamma(\mu, \nu)} \int_{\mathcal{P}(\Omega) \times \mathcal{P}(\Omega)} \|x_1 - x_2\|^2 d\gamma(x_1, x_2) \right)^{\frac{1}{2}}.$$

This metric is defined for any pair of probability measures μ and ν , both possessing finite second moments, and it involves the set $\Gamma(\mu, \nu)$, which encompasses all possible couplings of μ and ν . Previous studies have highlighted that the Wasserstein metric endows the probability space with a rich geometric structure (Malasto and Feragen, 2017; Takatsu, 2011; Villani, 2021). This geometric perspective is particularly beneficial in various applications, such as distributionally-robust optimization, where Wasserstein balls play a crucial role (Blanchet et al., 2019; Duchi et al., 2023; Esfahani and Kuhn, 2015; Gao and Kleywegt, 2023; Luo and Mehrotra, 2019; Pflug and Wozabal, 2007; Rahimian and Mehrotra, 2022; Sinha et al., 2017). Further, by applying the Kantorovich-Rubinstein duality, we can derive the dual formulation of the 2-Wasserstein distance, as detailed in **Theorem 1**. This dual formulation offers well-established interpretations in the context of optimal transport theory (Ambrosio et al., 2005; Panaretos and Zemel, 2019).

Theorem 1 (Dual representation; Benamou and Brenier (2000)). *The dual representation for \mathcal{W}_2 is given by*

$$\mathcal{W}_2^2(\mu, \nu) = 2 \sup_{u, v} \left\{ \int u d\mu + \int v d\nu \mid u(x) + v(y) \leq \frac{1}{2}|x - y|^2 \right\}.$$

The dual formulation enables the derivation of efficient and potentially closed-form solutions by employing standard methods from the field of convex optimization (Finlay et al., 2020).

2.2 First Variation

The Radon space, as defined on $\mathcal{P}(\Omega)$, inherently supports representations in terms of density. Consequently, moving forward, we will represent each element within this space using probability densities p .

The first variation of a functional \mathcal{F} on $\mathcal{P}(\Omega)$ is represented by a linear functional $\frac{\delta \mathcal{F}}{\delta p}$. This functional characterizes the response of \mathcal{F} to any feasible perturbation $h = p_1 - p_2$, where $p_1, p_2 \in \mathcal{P}(\Omega)$. Mathematically, this is expressed as follows:

$$\left. \frac{d}{dt} \mathcal{F}(p + th) \right|_{t=0} = \int \frac{\delta \mathcal{F}}{\delta p}(p) h(x) dx,$$

with t being a perturbation parameter. Essentially, this definition serves as a linear approximation, capturing how \mathcal{F} changes in response to minor alterations in its arguments.

It is important to note that the first variation is fundamentally the Gateaux derivative of the functional. By setting this first variation to zero, one essentially identifies the stationary points of the functional. This process is analogous to finding points where the gradient vanishes in standard calculus (Jordan et al., 1998). Techniques involving the first variation, such as the use of influence functions in causal inference, are prevalent in various mathematical and statistical applications (Cai et al., 2023; Kennedy, 2022; Tsiatis, 2006; Van Der Laan and Rubin, 2006).

2.3 Wasserstein Gradient Flows

Our focus is on identifying a trajectory through the space of probability measures, $\mathcal{P}(\Omega)$, that minimizes a functional $\mathcal{F} : \mathcal{P}(\Omega) \rightarrow \mathbb{R}$. This functional \mathcal{F} is characterized by its lower semi-continuity and boundedness from below. Additionally, the trajectory must maintain a certain level of smoothness. In this context, the Wasserstein gradient flow provides a framework for understanding the dynamics of probability measures. It describes how these measures evolve along the path

of steepest descent with respect to the functional \mathcal{F} , guided by the Riemannian metric imparted by the 2-Wasserstein metric, as discussed in Fan et al. (2021) in their variational approach.

Intuitively, this process involves iteratively updating the probability measure at each step n in the space $\mathcal{P}(\Omega)$, as expressed in the following equation:

$$p_\tau^{(n+1)} \in \arg \min_p \mathcal{F}(p) + \frac{\mathcal{W}_2^2(p, p_\tau^{(n)})}{2\tau}, \quad (1)$$

while taking the limit $\tau \rightarrow 0$. The following theorem illustrates the underlying mathematical principles governing the gradient flow for the minimization problem in the induced probability space.

Theorem 2 (Villani (2021)). *The gradient flow that addresses the continuous-time minimization problem in Eq. (1) is described by the Fokker-Planck equation*

$$\frac{dp}{dt} = \nabla \cdot \left(p \nabla \frac{\delta \mathcal{F}}{\delta p} \right), \quad (2)$$

where $\frac{\delta \mathcal{F}}{\delta p}$ represents the first variation of \mathcal{F} .

Theorem 2 states that the evolution of probability measures (denoted by p) that most steeply decreases the functional \mathcal{F} can be described by the Fokker-Planck equation, a partial differential equation that characterizes how the probability density function changes over time.

3 NORMALIZING WASSERSTEIN FLOWS

The evolution in **Theorem 2** naturally leads to the consideration of continuous normalizing flows (CNFs) as a powerful tool for modeling complex distributions, which are a class of generative models that aim to transform a simple base distribution into a more intricate target distribution through a smooth and invertible mapping, as delineated in Chen et al. (2018).

Given an ODE neural network defined as

$$\frac{dz}{dt} = f(z, t; \theta), \quad (3)$$

the change in log-density is governed by the differential equation representing the instantaneous change of variables:

$$\frac{\partial \log p(z(t))}{\partial t} = -\nabla \cdot f. \quad (4)$$

Alternatively, even in the presence of a Fokker-Planck or Liouville PDE for the system’s evolution, Eq. (4) can still be recovered (as shown by Chen et al. (2018), Eq. (32)) by tracking the trajectory of a particle $z(t)$ rather than examining $p(\cdot, t)$ at a fixed point.

Following the approach of Chen et al. (2018, 2020); Grathwohl et al. (2018), continuous normalizing flows are trained to maximize the terminal log-likelihood at t_1 , which is also a learnable parameter:

$$\log p(z(t_1)) = \log p(z(t_0)) - \int_{t_0}^{t_1} \nabla \cdot \left(\frac{\partial f}{\partial z} \right) dt. \quad (5)$$

This framework is numerically tractable thanks to the well-established adjoint method (Pontryagin, 2018) and stochastic trace estimators (Adams et al., 2018; Hutchinson, 1989).

The following figures show two basic continuous normalizing flows, originating from a prior distribution at $t = 0$ (typically a standard Gaussian), and evolving into a distribution parameterized by neural networks that aligns with the observed data.

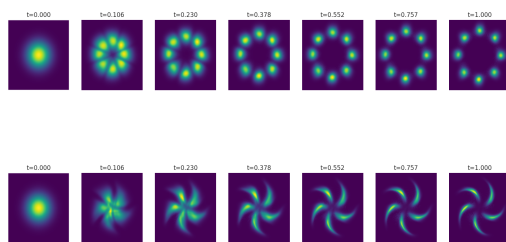


Figure 1: Illustration of Trajectories in Continuous Normalizing Flows: This figure presents the evolution of continuous normalizing flows from a 2-dimensional standard Gaussian prior to distinct data distributions. Specifically, the trajectories are shown for transformations leading to the data distributions generated by two datasets: the 8GAUSSIANS dataset and the PINWHEEL dataset, respectively.

The key aspect of CNFs is the use of neural networks to parameterize the velocity field in a differential equation, thereby enabling the model to learn complex transformations. In the realm of gradient flows, CNFs can be effectively utilized to approximate the dynamics described by the Fokker-Planck equation in Eq. (2). By leveraging the concept of the Wasserstein gradient flow, one can guide the CNFs to match the evolution of probability measures as governed by the functional \mathcal{F} . We term such flows as the *normalizing Wasserstein flows*. To achieve this, we propose adapting the CNFs to explicitly mimic the Wasserstein gradient flow, which involves two main components:

- Optimizing the CNF parameters to minimize the discrepancy between the modeled distribution and the target distribution.
- Ensuring the invertibility and smoothness of the CNF, which is critical for maintaining the prop-

erties of the probability measures throughout the normalizing Wasserstein flows.

The initial goal of aligning the learned probability density with the data distribution can be effectively accomplished, for instance, through maximum likelihood estimation. In this process, the probability density generated by the latent variables z is progressively trained to closely approximate the data distribution. This alignment ensures that the model captures the underlying structure and variability present in the data.

However, the second objective diverges from simply focusing on the behavior of the learned probability density. Instead, it concentrates on aligning the gradients of the density evolutions. This concept forms the crux of diffusion models, which emphasize the alignment of the neural network with the score (gradient) of the probability distributions. In certain structured scenarios, this alignment is achieved through well-defined stochastic interpolants (Albergo and Vandeneijnden, 2022; Albergo et al., 2023a,b). What becomes paramount in these cases is not the density itself, but the gradient flow matching (Lipman et al., 2022), which is central to the second objective.

In the context of stochastically interpolating between the noisy prior p_0 and the data distribution p_1 , the importance of this approach becomes evident in scenarios where there is an inclination to edge closer to the prior distribution, perceived as the “truth”, and move slightly away from a potentially biased data distribution. This shift can be particularly relevant in fields like causal inference or semiparametric literature, where understanding and approximating the underlying truth is crucial. In such cases, using an interpolated point between the prior and data distributions as a proxy becomes a strategic approach. This method enables researchers to balance the innate biases present in the data with the theoretical constructs of the prior distribution. By judiciously selecting a point on the continuum between p_0 and p_1 , one can effectively create a model that is not overly influenced by the idiosyncrasies of the observed data, while still retaining a connection to the empirical reality that the data represents (Kennedy, 2022; Van Der Laan and Rubin, 2006).

Stochastic interpolation thus fulfills a dual role. First, it acts as a vital mechanism to counteract data biases, adeptly integrating the theoretical insights gleaned from the prior distribution. This integration is key in ensuring that the final analysis is not overly skewed by anomalies or specific trends in the dataset. Second, it enables a more sophisticated exploration of the data generation process, grounded in theory. This explo-

ration goes beyond surface-level observations, delving into the deeper, underlying mechanisms that drive the data.

Building on these principles, we propose a methodology for achieving geometry-aware interpolation. This method is designed to optimize causal inference, adhering to the principles of semiparametric efficiency. By incorporating geometrical considerations into the interpolation process, we aim to refine our understanding of the data’s structure and causal relationships. This approach not only aligns with the theoretical framework but also enhances the practical effectiveness of causal inference, ensuring that the conclusions drawn are both statistically sound and relevant to the real-world phenomena they aim to explain.

3.1 Motivating Example: Variance Regularization

In the pursuit of learning a smooth distribution, one approach involves controlling its variance or its surrogates (Namkoong and Duchi, 2017). This is achievable by converting the distribution into a standard normal form using continuous normalizing flows and adding a penalty on its variance. We introduce a novel objective that integrates a variance regularization term with the initial loss function, aiming to control the distribution’s variance. We present a theorem describing the evolution of the log density under the associated Wasserstein gradient flow.

Theorem 3. *Operating on the space of zero-mean densities, i.e.,*

$$\int_{\mathbb{R}^n} zp(z) dz = 0,$$

the Wasserstein gradient flow, aimed at minimizing the variance functional

$$\mathcal{F}(p) = \frac{1}{2} \int_{\mathbb{R}^n} z^2 p(z) dz,$$

is described by the partial differential equation

$$\frac{\partial \log p}{\partial t} = \mathbf{1} + (\nabla \cdot \log p)z.$$

Proof. Observe that the functional $\mathcal{F}(p)$ is a linear functional. Moreover, it is bounded from below by 0, i.e., $\mathcal{F}(p) \geq 0$ for all permissible values of p . Consider any feasible perturbation $h = p_1 - p_2$ where $p_1, p_2 \in \mathcal{P}(\Omega)$. It is evident that

$$\int_{\mathbb{R}^n} h dz = \int_{\mathbb{R}^n} p_1 dz - \int_{\mathbb{R}^n} p_2 dz = 0.$$

We compute the first variation of \mathcal{F} by identifying $\frac{\delta\mathcal{F}}{\delta p}$ such that for any feasible h :

$$\begin{aligned} \int_{\mathbb{R}^n} \frac{\delta\mathcal{F}}{\delta p}(p)h \, dz &= \left. \frac{d}{dt} \mathcal{F}(p + th) \right|_{t=0} \\ &= \left. \frac{d}{dt} \frac{1}{2} \int_{\mathbb{R}^n} z^2(p + th) \, dz \right|_{t=0} \\ &= \frac{1}{2} \int_{\mathbb{R}^n} z^2 h \, dz, \end{aligned}$$

or

$$\frac{\delta\mathcal{F}}{\delta p}(p(z)) = \frac{1}{2} z^2,$$

and its gradient

$$\nabla \frac{\delta\mathcal{F}}{\delta p}(p(z)) = z.$$

The result then follows by substituting into the Fokker-Planck equation in Eq. (2):

$$\begin{aligned} \frac{\partial p(z)}{\partial t} &= \nabla \cdot \left(p \nabla \frac{\delta\mathcal{F}}{\delta p} \right) = \nabla \cdot (pz) \\ &= p \nabla \cdot z + z \nabla \cdot p = p \mathbf{1} + (\nabla \cdot p)z, \end{aligned}$$

and applying the partial derivatives to the log-likelihood. \square

In the course of our analysis, it becomes evident that the drift component in the Fokker-Planck equation exhibits a direct proportionality to the variable z . This observation implies a temporal dynamic where the probability mass is increasingly centralized around zero. The lack of a diffusion term further accentuates this behavior, as it precludes the dispersion of the probability mass, thereby catalyzing the convergence to a Dirac delta distribution at zero. Consequently, this dynamic inherently favors probability distributions characterized by diminishing variance over time.

To mitigate potential mode collapse, a phenomenon where the distribution narrows down to a point mass (Che et al., 2016; Salimans et al., 2016), our approach integrates actual data into the optimization objective. Drawing inspiration from the domain of physics-informed neural networks (Cai et al., 2021; Karniadakis et al., 2021), we incorporate a variance regularization term into the loss function. The modified loss function $\tilde{\mathcal{L}}$, parametrized by θ and evaluated at time t_1 , is formulated as:

$$\begin{aligned} \tilde{\mathcal{L}}(\theta, t_1; z) \\ = \mathcal{L}(z(t_1)) + \lambda \mathbb{E} \left\| \frac{\partial \log p(z)}{\partial t} - \mathbf{1} - (\nabla \cdot \log p)z \right\|_{\ell_2}^2, \end{aligned}$$

where λ represents the regularization coefficient. This formulation intuitively utilizes the divergence of the

log-likelihood, indicative of regions with concentration or dispersion of the probability density, as a means to regularize the variance.

While this approach effectively employs the PDE residual loss as a regularization term, it introduces a complexity: the need for gradients of the log-likelihood relative to the latent variables z . This requirement can be computationally challenging or necessitate the use of finite difference methods and numerical gradients, as opposed to straightforward gradient updates on the parameter vector θ . In the subsequent section, we propose a generalized framework that circumvents this complexity by focusing solely on the alignment of gradients, or what may be termed as “velocity fields”.

3.2 General Formulation

Inspired by Appendix A2 of Chen et al. (2018), and recent developments in velocity-based diffusion models Albergo et al. (2023a), to simplify computations, Eq. (4) suggests focusing the regularization on the velocity field $-f$ in the loss function. This is supported by the following theorem.

Theorem 4. *Suppose the Liouville equation characterizes the density evolution at a fixed point z^* as follows:*

$$\frac{\partial p(z^*, t)}{\partial t} = \nabla \cdot \left(p(z^*, t) \nabla \frac{\delta\mathcal{F}}{\delta p}(z^*, t) \right).$$

The conditions of Eq. (3) and (4) in the neural ODE framework are satisfied when the following velocity field alignment holds:

$$\frac{dz}{dt} + \nabla \frac{\delta\mathcal{F}}{\delta p} = 0. \quad (6)$$

Proof. By tracking the particle trajectory $z(t)$ instead of evaluating p at z^* and applying the chain rule, we obtain:

$$\begin{aligned} \frac{\partial p(z(t), t)}{\partial t} &= p_1(z(t), t) \frac{\partial z(t)}{\partial t} + p_2(z(t), t) \\ &= \sum_i \frac{\partial p(z(t), t)}{\partial z_i(t)} \frac{\partial z(t)}{\partial t} + p(z(t), t) \nabla \cdot \nabla \frac{\delta\mathcal{F}}{\delta p}(z(t), t) \\ &\quad + \sum_i \frac{\partial p(z(t), t)}{\partial z_i(t)} \nabla_i \frac{\delta\mathcal{F}}{\delta p}(z(t), t) \\ &= p(z(t), t) \nabla \cdot \nabla \frac{\delta\mathcal{F}}{\delta p}(z(t), t) \\ &= p(z(t), t) (-\nabla \cdot f(z(t), t)), \end{aligned}$$

leading to the equation:

$$\frac{\partial \log p(z(t))}{\partial t} = -\nabla \cdot f.$$

\square

This theorem ensures proximity to $\nabla \frac{\delta \mathcal{F}}{\delta p}$. This formulation incorporates the geometry induced by a generic functional \mathcal{F} , while also maximizing the likelihood of observed data. Accordingly, Eq. (6) yields a natural loss function defined as:

$$\tilde{\mathcal{L}}(\theta, t_1; z) = \mathcal{L}(z(t_1)) + \lambda \mathbb{E} \left\| \frac{dz}{dt} + \nabla \frac{\delta \mathcal{F}}{\delta p} \right\|_{\ell_2}^2. \quad (7)$$

When \mathcal{F} is the variance functional, the density evolution from t_0 to t_1 aims at minimizing variance. Conversely, when moving backward in time, the prior density (e.g., a standard normal distribution) evolves towards maximizing variance while maintaining a high likelihood.

Remarkably, the framework we propose here does not only work for variance regularization. Alternative geometry could be induced as well, such as regularization based on expectations or negative entropy, where the latter is often well-motivated by the heat equations.

3.3 Interpretations

This section elucidates two distinct interpretations of the loss function as defined in Eq. (7), aiming to elucidate the inherent trade-offs. These interpretations will serve as a foundation for more in-depth analysis in future works.

In a more formal exposition, consider a stochastic interpolant $X_t \sim p_t$ that smoothly transitions between $X_0 \sim p_0$ and $X_1 \sim p_1$, adhering to the requisite boundary conditions (Albergo et al., 2023a). The interpolant is defined as:

$$X_t = I(t, X_0, X_1) + \gamma(t)\epsilon \quad (8)$$

where ϵ represents a standard Gaussian noise, assumed to be independent of all other variables. To alleviate notational complexity, we set $t_0 = 0$ and $t_1 = 1$ without loss of generality.

3.3.1 Optimal Transport Interpretation

This interpretation principally engages with optimal transport theory. In the limit as the regularization coefficient $\lambda \rightarrow \infty$, the model asymptotically approaches a pure optimal transport framework. This convergence embodies the geometric principles underpinning Wasserstein gradient flows, as explicated in (Villani, 2021). A central element of this interpretation is the incorporation of the Benamou–Brenier formulation, which conceptualizes the optimal transport problem via velocity fields (Benamou and Brenier, 2000).

Let $p(t, z)$ denote the density function of $I(t, X_0, X_1)$ in Eq. (8), or equivalently, the density of X_t when the

diffusion term is $\gamma(t) = 0$. The boundary conditions are established as:

$$p(0, z) = p_0(z), \quad p(1, z) = p_1(z).$$

Introduce the Lagrangian coordinates $\mathbf{X}(t, z)$, defined by the relation:

$$\frac{\partial \mathbf{X}}{\partial t}(t, z) = -\nabla \frac{\delta \mathcal{F}}{\delta p}(t, \mathbf{X}(t, z)), \quad \mathbf{X}(0, z) = z.$$

Here, mass conservation is articulated through the pushforward equation:

$$\mathbf{X}(t, \cdot)_{\#} p_0 = p(t, \cdot), \quad (9)$$

which establishes a feasible transport map. In this context, “feasibility” implies that

$$\begin{aligned} & \mathcal{W}_2^2(p_0, p_1) \\ & \leq \int_{\mathbb{R}^n} p_0(z) \|\mathbf{X}(1, z) - z\|_{\ell_2}^2 dz \\ & = \int_{\mathbb{R}^n} p_0(z) \|\mathbf{X}(1, z) - \mathbf{X}(0, z)\|_{\ell_2}^2 dz \\ & = \int_{\mathbb{R}^n} p_0(z) \left\| \int_0^1 \frac{\partial \mathbf{X}}{\partial t}(t, z) dt \right\|_{\ell_2}^2 dz \\ & \leq \int_{\mathbb{R}^n} \int_0^1 p_0(z) \left\| \frac{\partial \mathbf{X}}{\partial t}(t, z) \right\|_{\ell_2}^2 dt dz \\ & = \int_0^1 \int_{\mathbb{R}^n} p_0(z) \left\| \nabla \frac{\delta \mathcal{F}}{\delta p}(t, \mathbf{X}(t, z)) \right\|_{\ell_2}^2 dz dt \\ & = \int_0^1 \int_{\mathbb{R}^n} p(t, z) \left\| \nabla \frac{\delta \mathcal{F}}{\delta p}(t, z) \right\|_{\ell_2}^2 dz dt \\ & = \int_0^1 \mathbb{E} \left\| \nabla \frac{\delta \mathcal{F}}{\delta p} \right\|_{\ell_2}^2 dt, \end{aligned}$$

where the penultimate equality is derived from Eq. (9). It is important to note that the equalities from above are attainable (Benamou and Brenier, 2000) under the condition

$$\nabla \frac{\delta \mathcal{F}}{\delta p} = (\mathbf{I} - \mathbf{T})((1-t)\mathbf{I} + t\mathbf{T})^{-1}.$$

Here, $\mathbf{X}(1, z) = T(z)$ represents the optimal transport map facilitating the transition from the initial distribution p_0 to the target distribution p_1 .

However, this formulation, in its rudimentary form, overlooks the intrinsic data structure, which is otherwise encapsulated in the first term $\mathcal{L}(z(t_1))$ through approaches such as maximum likelihood estimation. This term can be reinterpreted as an optimal transport objective but with an alternative cost function. Such a function might incorporate structured priors

(Alvarez-Melis et al., 2018) or domain-specific knowledge (Chuang et al., 2023). Importantly, when considering the geometry induced by $\mathcal{L}(z(t_1))$, assuming convexity is reasonable. This assumption is underpinned by constraining the normalizing flows to a class of functions that exclusively parameterize convex functions via neural networks (Alvarez-Melis et al., 2021). Additionally, this term can be viewed as a disruptor to the pure Wasserstein geometry, as posited by the Kantorovitch formulation. This disruption might be analogous to the Gromov-Wasserstein geometry (Sturm, 2006) or its regularizers (Vayer et al., 2018), which juxtapose distributions along normalizing Wasserstein flows against actual data distributions situated in disparate metric spaces.

3.3.2 Diffusion Equilibrium Interpretation

The second interpretation relates to the stationary distributions of two stochastic processes. The first process is characterized by ODE neural networks or diffusion models, tailored to empirical data as reflected in $\mathcal{L}(z(t_1))$. The second process adheres to flows or diffusions that precisely respect the Wasserstein geometry. In essence, the objective seeks to synergize the minimizers of these divergent objectives (Albergo et al., 2023a), fostering a balance between empirical data fidelity and geometric congruence.

In the context of Eq. (8), the gradient of the first variation $\nabla \frac{\delta \mathcal{F}}{\delta p}$ is identified as the unique minimizer of a specific quadratic objective (Albergo et al., 2023a):

$$\nabla \frac{\delta \mathcal{F}}{\delta p} = \arg \min_v \int_0^1 \mathbb{E} \left[\frac{1}{2} \|v(t, X_t)\|^2 + \left(\frac{\partial}{\partial t} I(t, X_0, X_1) + \dot{\gamma}(t)\epsilon \right) \cdot v(t, X_t) \right] dt.$$

Analogously, the time derivative of the latent variable z , $\frac{dz}{dt}$, is also characterized as the unique minimizer of a related quadratic objective. The alignment between these two velocity fields, namely $\nabla \frac{\delta \mathcal{F}}{\delta p}$ and $\frac{dz}{dt}$, is achieved through a synthesis of the two quadratic objectives. This synthesis provides a variational foundation for Eq. (7), effectively bridging the conceptual gap between stochastic interpolants and the optimization problem at hand.

4 OPTIMAL CAUSAL INFERENCE VIA OPTIMAL TRANSPORT

This section elaborates on the potential applications of causal inference, particularly focusing on addressing the disparity between sample and population distributions that often leads to biased estimation of pop-

ulation parameters. A typical scenario involves estimating the proportion of comments about specific underrepresented populations in a dataset where highly toxic comments might be censored, thereby never appearing in the dataset. This situation is further compounded by substantial distribution shifts, as identified by Koh et al. (2021), introducing additional bias in the estimation process.

Traditional statistical methods have been developed to adjust for this selection bias, notably including Inverse-Propensity Weighting (IPW) (Rosenbaum and Rubin, 1983, 1984) and G-methods (Robins, 1986). However, these methods often suffer from inefficiencies and can lead to erroneous conclusions, particularly when the underlying parametric models are misspecified. In contrast, semiparametric efficiency can be more reliably achieved through methods like Targeted Maximum Likelihood Estimation (TMLE) (Van Der Laan and Rubin, 2006; Van der Laan et al., 2011) and Augmented IPW (AIPW) (Robins et al., 1994; Robins and Rotnitzky, 1995; Scharfstein et al., 1999). These doubly robust methods, enhanced by nuisance estimators from deep learning and machine learning (Chernozhukov et al., 2018) and cross-fitting, offer an optimal bias-variance tradeoff for the target parameter in semiparametric or nonparametric models (Schuler and Rose, 2017). This tradeoff is asymptotically optimal as the variance of the target parameter estimate approaches the variance of the influence function (Kennedy, 2022), thus correcting the first-order bias.

Building upon the foundational concepts of optimal transport and Wasserstein gradient flows, as previously discussed, this section delves deeper into their application within the realm of causal inference. **Theorem 4**, as established earlier, proposes an innovative method of integrating normalizing flows with an optimally directed approach to achieve minimal variance in causal inference models. This section further explores the role of information geometry, particularly in enhancing the semiparametric Cramér-Rao lower bound. By harnessing the principles derived from optimal transport theory, we endeavor to develop causal inference methodologies that not only adhere to the principles of minimal variance in finite-sample settings but also compare favorably against traditional methods like TMLE and AIPW, which primarily emphasize asymptotic optimality.

4.1 Target Functional and Parametric Submodels

Consider a sequence of statistical models $\mathcal{M} = \{p_t\} \subset \mathcal{P}(\Omega)$ indexed by $t \in [0, \infty)$, where the score function g is characterized by zero mean and bounded variance with respect to the true density p_0 . This setup as-

sumes Hellinger differentiability—a key regularity condition—restricted to a locally asymptotic normal family where the score function is well-defined:

$$\int \left(\frac{\sqrt{p_t} - \sqrt{p_0}}{t} - \frac{1}{2} g_0 \sqrt{p_0} \right)^2 dz \rightarrow 0 \text{ as } t \rightarrow 0. \quad (10)$$

Targeted Maximum Likelihood Estimation (TMLE) identifies a least favorable parametric sub-model (van der Laan, 2017) that encompasses the true density p_0 (Stein et al., 1956). This is achieved through an initial estimator of the data distribution p_1 , subsequently refined to identify the optimal index within the parametric submodel:

$$p_t = p_0(1 + t g_0).$$

Consequently, we derive that

$$g_0 = \left. \frac{\partial}{\partial t} \log p_t \right|_{t=0}$$

is the score at the ground truth, a direct implication from Eq. (10), as demonstrated in Lemma 7.6 of Van der Vaart (2000).

In the realm of causal inference, our interest lies in evaluating a *target functional* $\psi : \mathcal{M} \rightarrow \mathbb{R}^d$ at the true measure $\psi(p_0)$. For instance, under the assumptions of positivity and censoring at random (Kennedy, 2022), the target functional for mean response can be defined as an expected regression functional

$$\psi(p) = \mathbb{E}_p[Y] = \mathbb{E}_p[\mathbb{E}_p[Y | A = 1, X]]$$

evaluated at $p = p_0$.

4.2 Local Semiparametric Efficiency

To elucidate the first-order bias in a misspecified model p_t , we employ the von Mises expansion (or distributional Taylor expansion) at the true model p_0 (Fernholz, 2012):

$$\psi(p_t) - \psi(p_0) = \int \varphi(p_0)(p_t - p_0) dx + R_2(p_t, p_0),$$

where φ represents the efficient influence function.

Considering Neyman orthogonality (Chernozhukov et al., 2018, 2022), and assuming pathwise differentiability of the target functional $\psi(p_t)$, we have:

$$\frac{d}{dt} \psi(p_t) = \langle \varphi(p_t), g_t \rangle_{p_t},$$

with a generic score

$$g_t = \left. \frac{\partial}{\partial t} \log p_t \right|_{p_t} \in \mathcal{T}_{p_t} \mathcal{M}. \quad (11)$$

Thus, in estimating a statistical functional $\psi(p_t)$ at $t = 0$, the tightest semiparametric Cramér-Rao lower bound is expressed as:

$$\begin{aligned} \sup_{g_0 \in \mathcal{T}_{p_0} \mathcal{M}} \frac{\left(\left. \frac{d}{dt} \psi(p_t) \right|_{t=0} \right)^2}{\langle g_0, g_0 \rangle_{p_0}} &= \sup_{g_0 \in \mathcal{T}_{p_0} \mathcal{M}} \frac{\langle \varphi(p_0), g_0 \rangle_{p_0}^2}{\langle g_0, g_0 \rangle_{p_0}} \\ &\leq \langle \varphi(p_0), \varphi(p_0) \rangle_{p_0} \\ &= \text{Var}(\varphi(p_0)), \end{aligned}$$

where equality is achieved at $g_0 = \varphi(p_0) \in \mathcal{T}_{p_0} \mathcal{M}$, following the Cauchy-Schwarz inequality. Apparently, for $t = 0$, we have the Cramér-Rao lower bound, which shows that the efficiency is achieved when the score function g_0 is equal to the efficient influence function $\varphi(p_0)$. This congruence signifies an optimal estimation under certain regularity conditions. Nevertheless, as we extend our consideration to a general t , the task of identifying an efficient influence function $\varphi(p_t)$, such that it consistently resides within the tangent space $\mathcal{T}_{p_t} \mathcal{M}$ of the model manifold \mathcal{M} , becomes arduous. The complexity of this problem escalates due to the dynamic nature of the tangent space, which evolves as the model p_t changes.

The score function g_t , defined in Eq. (11) as the derivative of the log-likelihood with respect to the parameter at p_t , captures only the *local* sensitivity of the model at this point. In contrast, the efficient influence function $\varphi(p_t)$, apart from encapsulating this local sensitivity, also embodies the capacity to reflect the *global* structural intricacies of the statistical model. This global perspective is critical in relation to the target functional ψ , which the efficient influence function aims to estimate.

Given this context, the concept of semiparametric efficiency appears inherently local. A pertinent query then emerges: Is it feasible to pursue global semiparametric efficiency? One promising approach is to minimize the semiparametric efficiency bound over the entire trajectory of the model manifold \mathcal{M} . This minimization can be conceptualized through the framework of normalizing Wasserstein flows. Specifically, the Wasserstein gradient flows, designed to minimize the Cramér-Rao lower bound, incorporate considerations of the global structural attributes of the model. Formally, the objective is to minimize the functional:

$$\mathcal{F} = \text{Var}_{p_t}(\varphi(p_t)),$$

where \mathcal{F} represents the variance of the efficient influence function under the distribution p_t . This minimization can be operationalized by formulating a velocity regularization term, as delineated in Eq. (7), which governs the evolution of the flows.

4.3 Experiments

Consider a simple illustrative example where our objective is to estimate the target functional corresponding to the marginal population mean of a two-dimensional random variable $(X, \cdot) : \Omega \rightarrow \mathbb{R}^2$. The target functional in this context is defined as:

$$\psi(p) = \mathbb{E}_p[X].$$

The efficient influence function can be straightforwardly derived as:

$$\varphi(p) = X - \mathbb{E}_p[X].$$

In accordance with Eq. (7), we align the ODE neural network, represented by $f = \frac{dz}{dt}$, with the Wasserstein gradient flows. These flows are aimed at minimizing the functional $\mathcal{F} = \text{Var}_{p_t}(\varphi(p_t))$.

Suppose the true distribution p_0 is a standard Gaussian, which coincidentally also serves as the prior in continuous normalizing flows. The data distribution is characterized by p_1 , as depicted in Figure 1. For instance, in the case of the 8GAUSSIANS dataset, the marginal distribution of X is gradually subjected to finite-sample bias, as illustrated in the subsequent figure.

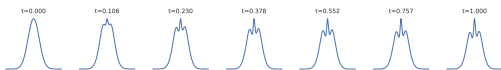


Figure 2: Illustrative Transition from Initial Noise to Biased Sample Distribution: This figure depicts the evolution of the first dimension in the 8GAUSSIANS dataset, starting from pure noise and gradually transitioning towards a biased sample distribution.

With varying degrees of regularization strength as specified in Eq. (7), we derive the normalizing Wasserstein flows that effectively bridge the true distribution p_0 and the data distribution p_1 . The subsequent figures visualize these flows for several toy datasets. Notably, the mean-squared error (MSE) associated with the normalizing Wasserstein flows is consistently lower than that of the naive flows, which lack regularization, at all points along the trajectory. This observation is crucial, as the finite-sample estimation error is fundamentally characterized by the MSE of plug-in estimators. Consequently, our analysis demonstrates the feasibility of more efficient estimators in finite-sample scenarios. Such estimators facilitate optimal causal inference, optimally positioned within the trajectory connecting p_0 and p_1 .

Figure 3 presents a dual analysis. The left panel illustrates the mean-squared error of plug-in estimators

along the flow path, while the right panel displays the variance of the efficient influence function. It is evident that each flow attains semiparametric efficiency at the true distribution p_0 . Notably, estimators with stronger velocity regularization demonstrate greater efficiency compared to those without any regularization.

The results in Figure 4 mirror those observed for the 8GAUSSIANS dataset, showcasing similar patterns in the efficiency and variance metrics for the studied flows.

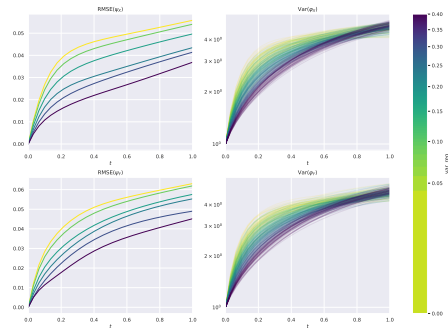


Figure 3: Analysis of Normalizing Wasserstein Flows on 8GAUSSIANS

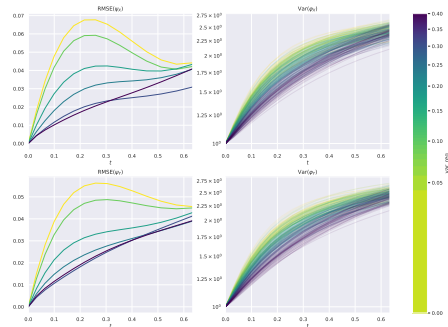


Figure 4: Consistent Outcomes in Normalizing Wasserstein Flows for PINWHEEL

5 CONCLUSIONS

In the conclusion, we summarize key findings and insights from our study.

First, TMLE effectively conducts interpolation between p_0 and p_1 by optimally fitting the index ϵ , achieving a state of zero bias. This method demonstrates precision in balancing the distributions, aligning closely with the theoretical ideal.

Second, our preliminary experimental results indicate that the RMSE of estimators based on interpolation could universally be lower than that of TMLE. This potential improvement may be attributed to the allowance for some level of bias, which, counterintuitively, can enhance overall accuracy.

Lastly, when equipped with oracle Riesz representers, which are the correctly specified perturbation directions of an initial statistical model, both TMLE and the C-Learner can precisely project onto a space where the efficient influence function has a zero empirical mean. This leads to asymptotic unbiasedness. In contrast, our approach involves an approximate projection of the data-inspired statistical model along a trajectory. This trajectory, which we define as the geometry-aware normalizing Wasserstein flows, is designed to attain semiparametric efficiency almost ubiquitously. It represents a sophisticated path that integrates geometrical insights with statistical efficiency, offering a nuanced and theoretically grounded approach to modeling and inference.

Acknowledgements

We express sincere gratitude to Mark Goldstein for his invaluable and insightful feedback on the nuanced interplay between velocity-based regularization and stochastic interpolants within diffusion models. Our appreciation also goes to Professor Santiago Balseiro for his expert advice on the intricacies of local linearization and a thorough analysis of global stability using Lyapunov functions. We extend our sincere appreciation to all contributors who participated in the 2023 Financial and Business Analytics Poster Session hosted by the Data Science Institute at Columbia University. The variety and depth of their insightful feedback have been pivotal in the enhancement and expansion of our research scope. Additionally, we are profoundly grateful for the valuable feedback provided by Dr. Sinho Chewi during the NeurIPS 2023 conference. His expertise and perspectives have significantly contributed to the refinement of our work.

References

- Adams, R. P., Pennington, J., Johnson, M. J., Smith, J., Ovadia, Y., Patton, B., and Saunderson, J. (2018). Estimating the spectral density of large implicit matrices. *arXiv preprint arXiv:1802.03451*.
- Albergo, M. S., Boffi, N. M., and Vanden-Eijnden, E. (2023a). Stochastic interpolants: A unifying framework for flows and diffusions. *arXiv preprint arXiv:2303.08797*.
- Albergo, M. S., Goldstein, M., Boffi, N. M., Ranganath, R., and Vanden-Eijnden, E. (2023b). Stochastic interpolants with data-dependent couplings. *arXiv preprint arXiv:2310.03725*.
- Albergo, M. S. and Vanden-Eijnden, E. (2022). Building normalizing flows with stochastic interpolants. *arXiv preprint arXiv:2209.15571*.
- Alvarez-Melis, D., Jaakkola, T., and Jegelka, S. (2018). Structured optimal transport. In *International conference on artificial intelligence and statistics*, pages 1771–1780. PMLR.
- Alvarez-Melis, D., Schiff, Y., and Mroueh, Y. (2021). Optimizing functionals on the space of probabilities with input convex neural networks. *arXiv preprint arXiv:2106.00774*.
- Ambrosio, L., Gigli, N., and Savaré, G. (2005). *Gradient flows: in metric spaces and in the space of probability measures*. Springer Science & Business Media.
- Benamou, J.-D. and Brenier, Y. (2000). A computational fluid mechanics solution to the monge-kantorovich mass transfer problem. *Numerische Mathematik*, 84(3):375–393.
- Blanchet, J., Kang, Y., and Murthy, K. (2019). Robust wasserstein profile inference and applications to machine learning. *Journal of Applied Probability*, 56(3):830–857.
- Cai, S., Mao, Z., Wang, Z., Yin, M., and Karniadakis, G. E. (2021). Physics-informed neural networks (pinns) for fluid mechanics: A review. *Acta Mechanica Sinica*, 37(12):1727–1738.
- Cai, T. T., Fonseca, Y., Hou, K., and Namkoong, H. (2023). C-learner: Constrained learning for causal inference. In *Conference on Digital Experimentation*.
- Che, T., Li, Y., Jacob, A. P., Bengio, Y., and Li, W. (2016). Mode regularized generative adversarial networks. *arXiv preprint arXiv:1612.02136*.
- Chen, R. T., Amos, B., and Nickel, M. (2020). Learning neural event functions for ordinary differential equations. *arXiv preprint arXiv:2011.03902*.

- Chen, R. T., Rubanova, Y., Bettencourt, J., and Duvenaud, D. K. (2018). Neural ordinary differential equations. *Advances in neural information processing systems*, 31.
- Chernozhukov, V., Chetverikov, D., Demirer, M., Duflo, E., Hansen, C., Newey, W., and Robins, J. (2018). Double/debiased machine learning for treatment and structural parameters.
- Chernozhukov, V., Escanciano, J. C., Ichimura, H., Newey, W. K., and Robins, J. M. (2022). Locally robust semiparametric estimation. *Econometrica*, 90(4):1501–1535.
- Chuang, C.-Y., Jegelka, S., and Alvarez-Melis, D. (2023). Infort: Information maximizing optimal transport. In *International Conference on Machine Learning*, pages 6228–6242. PMLR.
- Duchi, J., Hashimoto, T., and Namkoong, H. (2023). Distributionally robust losses for latent covariate mixtures. *Operations Research*, 71(2):649–664.
- Esfahani, P. M. and Kuhn, D. (2015). Data-driven distributionally robust optimization using the wasserstein metric: Performance guarantees and tractable reformulations. *arXiv preprint arXiv:1505.05116*.
- Fan, J., Zhang, Q., Taghvaei, A., and Chen, Y. (2021). Variational wasserstein gradient flow. *arXiv preprint arXiv:2112.02424*.
- Fernholz, L. T. (2012). *Von Mises calculus for statistical functionals*, volume 19. Springer Science & Business Media.
- Finlay, C., Jacobsen, J.-H., Nurbekyan, L., and Oberman, A. (2020). How to train your neural ode: the world of jacobian and kinetic regularization. In *International conference on machine learning*, pages 3154–3164. PMLR.
- Gao, R. and Kleywegt, A. (2023). Distributionally robust stochastic optimization with wasserstein distance. *Mathematics of Operations Research*, 48(2):603–655.
- Grathwohl, W., Chen, R. T., Bettencourt, J., Sutskever, I., and Duvenaud, D. (2018). Ffjord: Free-form continuous dynamics for scalable reversible generative models. *arXiv preprint arXiv:1810.01367*.
- Hutchinson, M. F. (1989). A stochastic estimator of the trace of the influence matrix for laplacian smoothing splines. *Communications in Statistics-Simulation and Computation*, 18(3):1059–1076.
- Jordan, R., Kinderlehrer, D., and Otto, F. (1998). The variational formulation of the fokker–planck equation. *SIAM journal on mathematical analysis*, 29(1):1–17.
- Karniadakis, G. E., Kevrekidis, I. G., Lu, L., Perdikaris, P., Wang, S., and Yang, L. (2021). Physics-informed machine learning. *Nature Reviews Physics*, 3(6):422–440.
- Kennedy, E. H. (2022). Semiparametric doubly robust targeted double machine learning: a review. *arXiv preprint arXiv:2203.06469*.
- Koh, P. W., Sagawa, S., Marklund, H., Xie, S. M., Zhang, M., Balsubramani, A., Hu, W., Yasunaga, M., Phillips, R. L., Gao, L., et al. (2021). Wilds: A benchmark of in-the-wild distribution shifts. In *International Conference on Machine Learning*, pages 5637–5664. PMLR.
- Lipman, Y., Chen, R. T., Ben-Hamu, H., Nickel, M., and Le, M. (2022). Flow matching for generative modeling. *arXiv preprint arXiv:2210.02747*.
- Liu, S., Li, W., Zha, H., and Zhou, H. (2022). Neural parametric fokker–planck equation. *SIAM Journal on Numerical Analysis*, 60(3):1385–1449.
- Luo, F. and Mehrotra, S. (2019). Decomposition algorithm for distributionally robust optimization using wasserstein metric with an application to a class of regression models. *European Journal of Operational Research*, 278(1):20–35.
- Mallasto, A. and Feragen, A. (2017). Learning from uncertain curves: The 2-wasserstein metric for gaussian processes. *Advances in Neural Information Processing Systems*, 30.
- Namkoong, H. and Duchi, J. C. (2017). Variance-based regularization with convex objectives. *Advances in neural information processing systems*, 30.
- Panaretos, V. M. and Zemel, Y. (2019). Statistical aspects of wasserstein distances. *Annual review of statistics and its application*, 6:405–431.
- Pflug, G. and Wozabal, D. (2007). Ambiguity in portfolio selection. *Quantitative Finance*, 7(4):435–442.
- Pontryagin, L. S. (2018). *Mathematical theory of optimal processes*. Routledge.
- Rahimian, H. and Mehrotra, S. (2022). Frameworks and results in distributionally robust optimization. *Open Journal of Mathematical Optimization*, 3:1–85.
- Raissi, M., Perdikaris, P., and Karniadakis, G. E. (2019). Physics-informed neural networks: A deep learning framework for solving forward and inverse problems involving nonlinear partial differential equations. *Journal of Computational physics*, 378:686–707.
- Robins, J. (1986). A new approach to causal inference in mortality studies with a sustained exposure period—application to control of the healthy

- worker survivor effect. *Mathematical modelling*, 7(9-12):1393–1512.
- Robins, J. M. and Rotnitzky, A. (1995). Semiparametric efficiency in multivariate regression models with missing data. *Journal of the American Statistical Association*, 90(429):122–129.
- Robins, J. M., Rotnitzky, A., and Zhao, L. P. (1994). Estimation of regression coefficients when some regressors are not always observed. *Journal of the American statistical Association*, 89(427):846–866.
- Rosenbaum, P. R. and Rubin, D. B. (1983). The central role of the propensity score in observational studies for causal effects. *Biometrika*, 70(1):41–55.
- Rosenbaum, P. R. and Rubin, D. B. (1984). Reducing bias in observational studies using subclassification on the propensity score. *Journal of the American statistical Association*, 79(387):516–524.
- Salimans, T., Goodfellow, I., Zaremba, W., Cheung, V., Radford, A., and Chen, X. (2016). Improved techniques for training gans. *Advances in neural information processing systems*, 29.
- Scharfstein, D. O., Rotnitzky, A., and Robins, J. M. (1999). Adjusting for nonignorable drop-out using semiparametric nonresponse models. *Journal of the American Statistical Association*, 94(448):1096–1120.
- Schuler, M. S. and Rose, S. (2017). Targeted maximum likelihood estimation for causal inference in observational studies. *American journal of epidemiology*, 185(1):65–73.
- Sinha, A., Namkoong, H., Volpi, R., and Duchi, J. (2017). Certifying some distributional robustness with principled adversarial training. *arXiv preprint arXiv:1710.10571*.
- Stein, C. et al. (1956). Efficient nonparametric testing and estimation. In *Proceedings of the third Berkeley symposium on mathematical statistics and probability*, volume 1, pages 187–195.
- Sturm, K.-T. (2006). On the geometry of metric measure spaces.
- Takatsu, A. (2011). Wasserstein geometry of gaussian measures.
- Tsiatis, A. A. (2006). Semiparametric theory and missing data.
- van der Laan, M. (2017). A generally efficient targeted minimum loss based estimator based on the highly adaptive lasso. *The international journal of biostatistics*, 13(2).
- Van der Laan, M. J., Rose, S., et al. (2011). *Targeted learning: causal inference for observational and experimental data*, volume 4. Springer.
- Van Der Laan, M. J. and Rubin, D. (2006). Targeted maximum likelihood learning. *The international journal of biostatistics*, 2(1).
- Van der Vaart, A. W. (2000). *Asymptotic statistics*, volume 3. Cambridge university press.
- Vayer, T., Chapel, L., Flamary, R., Tavenard, R., and Courty, N. (2018). Fused gromov-wasserstein distance for structured objects: theoretical foundations and mathematical properties. *arXiv preprint arXiv:1811.02834*.
- Villani, C. (2021). *Topics in optimal transportation*, volume 58. American Mathematical Soc.